Dynamics of GDOES-induced surface roughening in metal interfaces

R. Escobar Galindo · L. Vázquez

Abstract The roughness induced during glow-discharge optical-emission spectroscopy (GDOES) measurements has been reported to cause a loss of resolution during GDOES depth-profiling analysis. In this paper, we undertake for the first time a study of the dynamics of the surface morphology of chromium and titanium thin films (designed in mono and multilayer structures) under the impinging of GDOES incoming ions. We performed this study under the theoretical framework of the dynamic scaling theory, by analysing surface morphology changes, as measured ex-situ by AFM, with irradiation time. For single metal layers it was found that, after an initial surface smoothening, the surface undergoes a rapid steep roughening for both systems, with quite similar quantitative dynamics. Once this roughening ends a second temporal scaling regime arises, operating for long length scales with dynamics depending on the sputtering rate of the material. For the chromium layer, with a very high sputtering rate of 5.5 μm min^{-1}, this regime is consistent with the KPZ model, whereas for the titanium layer an EW scaling regime is indicated. These different scaling regimes are consistent with the development of larger surface slopes for the Cr system. In the multilayer systems, the initial roughness induced on the top Cr layer by GDOES has similar dynamics to that for single-layer Cr. However, a clear decrease in the roughness was observed once the underlying Ti layer, with a lower sputtering rate, was reached. This decrease in the induced roughness is maintained while the Ti layer is eroded. Therefore, choice of appropriate material (i.e. sputtering yield values) combinations and of their depth of location can enable tuning of GDOES-induced roughness and achieve substantial control over the depth profiling process.

Keywords Spectroscopy instrumentation · Thin films · AFM (atomic force microscopy) · Modeling

Introduction

Glow-discharge optical-emission spectroscopy (GDOES) has become a widely used technique [1, 2] that competes with more traditional and well-known analytical techniques, including AES, XPS, and SIMS [3–7]. During GDOES experiments, samples are isotropically sputtered by Ar^+ ions [8] and accelerated neutral species with high current flux (approximately 100 mA cm^{-1}) but very low energy (<50 eV). The sputtered atoms are then excited by the plasma and de-excited by photon emission with a characteristic wavelength, enabling element distinction. High sputtering rates, of more than 1 μm min^{-1}, are easily obtained, enabling fast measurements, typically of the order of seconds or a few minutes. GDOES has been used extensively in the study of depth profiling of thin (10–100 nm) and ultrathin (<10 nm) films [9–13], although a serious loss of resolution with depth during GDOES analysis has been reported [14–18]. The major factors contributing to this loss of resolution are related to the high erosion rate, sample heating, changes to crater geometry during the sputtering process, and ion-induced surface roughening. The latter becomes highly detrimental for multilayer systems, because it results in the mixing of consecutive layers when the individual layer thickness is at the nanometer scale.

R. Escobar Galindo (✉) · L. Vázquez
Instituto de Ciencia de Materiales de Madrid (ICMM -CSIC),
Cantoblanco, 28049 Madrid, Spain
e-mail: rescobar@icmm.csic.es

Increased surface roughening with GDOES sputtering time is well documented in the literature. Works by Harrison et al. [19, 20] in the 70s already reported changes in the surface morphology of samples after GDOES sputtering. Shimizu et al. [21, 22] and Escobar Galindo et al. [23] revealed the effect of GDOES-induced roughening on the depth profiling of thin films. In the 90s Oswald et al. [24] and Präßler et al. [25] used deconvolution procedures to improve GDOES depth profiles by using information on crater formation. More recently, Escobar Galindo and Albella [26] proposed a simple model to interpret and predict the depth profiles of periodic multilayer structures with individual layer thickness in the range 10–100 nm, i.e. within the order of magnitude of roughness induced during depth profiling by GDOES. The model is based on the assumption that the surface roughening produced by the ion bombardment gives rise to partial mixing of the layers and their interfaces, leading to a smoothing of the otherwise abrupt profiles. Fitting experimental profiles for a set of samples made of alternating Ti and Cr layers of a wide range of thicknesses enables the degradation constant b (pre-exponential factor) for each material to be obtained. A novel aspect of this work is that the layer mixing at the interface is modulated by the sputtering rates of the adjacent materials.

In this study we analyse the changed target surface morphology induced by GDOES sputtering. Usually, such analysis has been limited to imaging the sample surface and evaluating the surface roughness. For example, in the excellent work of Malherbe et al. [27], a rigorous study of changes to the surface morphology of monocrystalline silicon wafers and chromate conversion coatings under the experimental GDOES conditions (sputtering time, discharge gas pressure, and power) was performed by atomic force microscopy (AFM) and roughness measurements. Trigoulet et al. [28] reported AFM and transmission electron microscopy (TEM) changes to the surface topography of anodic aluminium oxide films of different thickness under GDOES. Here our objective is to take study of this subject further, by characterizing the statistical properties of the irradiated surfaces from the AFM studies. More specifically, we have focused on the dynamics of the surface morphology under the impinging of the incoming ions. We have taken a fundamental approach by using dynamic scaling theory (DST) as the framework of our analysis. This theory focuses on the characterization of the surface roughness lateral correlations (i.e. how the roughness changes with the length scale) and time dynamics [29, 30]. When considering which variables must be changed to study the relationship between GDOES conditions and local (nanoscale) surface morphology, there are several options: the system pressure, power used, surface location on the irradiated area, and target configuration are good candidates for such study. However, to be able to analyze and properly interpret the data, the number of variables should be minimized because otherwise many effects can operate simultaneously, which impedes data analysis. Therefore, we characterized the surface morphology of different samples (see Experimental) for increasing treatment times, keeping the pressure and power constant. Also, we always studied the central spot of the irradiated area to avoid any possible dependence of the local surface morphology on the position within the circular bombarded zone. It was easy to focus on this spot because of the lateral screws and optical microscope incorporated into the AFM system. We then analyzed how the surface morphology depends on the ion dose; that is, we studied the surface morphology dynamics under GDOES. By changing the compositional configuration of the target and keeping the same conditions, we also studied how these dynamics depend on the target composition. It should be noted that to properly study the interface dynamics, it is necessary to sample relatively wide temporal windows. This becomes even more important when different dynamic regimes are present, as in this case (see below). For this reason, we produced quite thick films to enable us to follow the interface dynamics.

Experimental and methods

Coating deposition

Metallic chromium and titanium, and multilayers of alternating titanium and chromium films of different thickness were deposited on a three-inch silicon (100) substrate by DC magnetron sputtering in a high-purity (99.999 %) argon atmosphere using two sputtering sources, placed 6.5 cm away from the substrate holder. Details of the sputtering system have been described elsewhere [31]. The base pressure was approximately 2×10^{-4} Pa, and the working pressure was in the range 0.16–0.23 Pa. The cathode power was held at 100 W. No bias voltage was applied to the substrate holder by a DC power supply. The deposition rates of the specimens were 12.5 nm min^{-1} for titanium, and 25.0 nm min^{-1} for chromium. Table 1 gives a summary of the coatings studied in this work.

Coating characterization

GDOES depth profile analysis of the coatings was performed using a Horiba Jobin Yvon RF GD Profiler equipped with a

Table 1 Description of the thin films studied in this paper

Sample	Element	Thickness (μm)	Sputtering yield (μm min^{-1})	Sputtering time (s)	Roughness nm)
Cr monolayer	Cr	3	5.0	0	3.6±0.4
				1	2.4±0.2
				3	17±2
				5	30±3
				7	32±3
				10	33±3
				20.5	39±4
Ti monolayer	Ti	3	3.5	0	19±2
				2	9±1
				4	19±2
				6	25±3
				19	29±3
				34	35±4
Cr–Ti–Cr trilayer	Cr	0.5	5.0	0	3.4±0.3
				4	10±1
	Ti	0.5	3.5	9	5.8±0.6
				12	8.0±0.8
				15	6.6±0.7
	Cr	0.5	5.0	17	14±1
				19	12±1
				21	11±1
Cr–Ti thick bilayer	Cr	0.75	5.0	0	4.3±0.4
				4	9±1
				9	26±3
	Ti	2.25	3.5	12	12±1
				19	20±2
				24	17±2
				29	18±2
				34	19±2

4 mm diameter copper anode and operating in argon gas [1, 14]. In previous works [18, 23], Escobar Galindo et al. performed a complete optimisation of the operating conditions for analysis using this GDOES system. By using a radio frequency discharge pressure of 650 Pa and a forward power of 40 W, multilayers in the nanometre range could be analysed. Therefore, in this study these operation settings were used. Emission responses from the excited sputtered elements were detected using a polychromator of focal length 500 mm. The optical path of the spectrometer was nitrogen purged. The emission lines used were 288.158 nm for silicon, 365.35 nm for titanium, and 425.433 nm for chromium. The quantified spectra of silicon, titanium, and chromium were obtained using certified reference materials (A/8, CE650, CZ2011, JK41-1 N, N50.01, NSC3S, RA18/8, RC32/11, RC40/11, RH18/17, RH32/6, RNI15/14, RNI15/20, SS112, SS113, SS114, VAWE-4/5). A stoichiometric TiN coating (provided by the company Ceratizit) and a silicon (100) wafer were also introduced in the calibration lines, to obtain high contents of titanium and silicon, respectively. The chamber was cleaned by sputtering a silicon (100) sample for 20 min before the measurements. This procedure minimises surface contamination of samples from the source and enables faster stabilisation of the plasma and, therefore, a higher surface resolution of the GDOES set-up [7]. No memory effects were observed after this pre-sputtering procedure. GDOES discharges were performed on a series of spots in the samples for different sputtering times (see Table 1). The shape and depth of the craters and the coating thickness were measured by profilometry using a Dektak 3030 surface profilometer.

AFM measurements were performed on different areas at the middle of the GDOES crater in ambient conditions, using either a Nanoscope IIIa (Veeco, USA) or PicoPlus Agilent 5500 (Agilent, USA) in intermittent-contact operating

conditions, using silicon cantilevers (Veeco, USA) with a nominal radius of curvature of 8 nm. Images of different sizes, from less than 1 μm up to 20 μm, were taken. Statistical analysis of the images was performed using the software of both sets of equipment and the Gwyddion Free Software [32].

Dynamic scaling theory

As explained in the Introduction, the main analysis of this investigation was made within the framework of dynamic scaling theory (DST). DST has been successfully used to study the growth or etching of different surfaces [29, 33]. Here, we provide a brief explanation of the basic concepts needed to follow our study. The first assumption is that the growing surface, h, does not have overhangs, i.e., is a one-valued function $h(\boldsymbol{r},t)$, where $\boldsymbol{r}$ is a vector in the base plane, t is the deposition time, and $\langle h(t)\rangle$ is the mean height. The roughness or interface width (σ) is defined as the mean square deviation of the local height, h, with respect to the mean height $\langle h(t)\rangle$:

$$\sigma(t) = \left\langle [h(\boldsymbol{r},t) - \langle h(t)\rangle]^2 \right\rangle^{0.5} \quad (1)$$

where $\langle \ldots \rangle$ represents the average over all $\boldsymbol{r}$ within a given area.

Then, if standard Family–Vicsek dynamic scaling holds [34], there are specific scaling relationships of the temporal and spatial dependences of σ; for example, that referring to the evolution of the surface roughness with the bombardment time (t): $\sigma \propto t^{\beta}$. The growth exponent β can be determined by following the change of σ, which is directly obtained from large AFM images by the AFM software, with the irradiation time.

Another commonly used scaling relationship comes from the lateral correlations of the surface roughness obtained from the power spectral density (PSD) of the surface morphology. This function is defined as $PSD(k,t)=\langle H(\boldsymbol{k},t)H(-\boldsymbol{k},t)\rangle$, where $H(\boldsymbol{k},t)$ is the two-dimensional Fourier transform of $h(\boldsymbol{r},t)-\langle h(t)\rangle$, and k is the spatial frequency in the reciprocal space related to the lateral distance l ($k=1/l$). This radial averaging is relevant to isotropic surface morphologies, including those studied in this work. The PSD function also displays regions with scaling relationships as $PSD(k) \propto k^{-2(\alpha+1)}$, with a lower k_c cut-off that usually shifts to smaller k values as growth proceeds [29]. For $k<k_c$ a region of constant PSD is found, which corresponds to the absence of any surface correlation at the corresponding lengths. To better explain these concepts, Fig. S1 (see Electronic Supplementary Material) shows a typical PSD curve, obtained from an AFM image of a Cr film eroded by GDOES for 10 s. In this example, three main zones can be distinguished:

1. A first regime in which $\alpha_1=0.7$, which ends at the crossover k value of $k_{c1}\sim0.0027$ nm^{-1};
2. For smaller k values, there is a second regime where $\alpha_2=0.39$, which extends down to $k_{c2}\sim0.00085$ nm^{-1};
3. From this second crossover to smaller k values there is a more or less horizontal part of the PSD, which corresponds to the length scale ($1/k$) range for which there is no correlation between the height of two sites that are $1/k$ apart.

The roughness exponent α describes the horizontal correlations of the surface roughness for a given length-scale range. The existence of such correlation implies that the heights of every two points at the surface within this scale range are not independent (i.e. are correlated). Hence, one can extract the value of α at the corresponding length scales from a logarithmic plot of the PSD versus k [33]. From the temporal change of the typical lateral-surface correlation length, $\xi=1/k_c$, a behaviour $\xi \propto t^{1/z}$ follows, where $1/z$ is the coarsening exponent describing the lateral increase of the region in which the surface heights are correlated. The PSD also provides valuable information on the length scales at which roughening or smoothening processes take place, as will be revealed for our systems. The surface roughness (σ) is related to the PSD function through the expression:

$$\sigma^2 = 2\pi \int k \; PSD(k)\, dk \quad (2)$$

When so-called kinetic roughening occurs, the three exponents are related as $1/z=\beta/\alpha$ [29]. Another indicator of the presence of scaling properties is that, for increasing growth (etching) times, the linear region defining the α value in the logarithmic plot increases its extent—as commented above—but all PSD curves overlap at those parts already defined for shorter times. These exponents are related to the operating mechanisms that determine the statistical properties of the surface morphology. Thus, by analysing the surface morphology through determining the scaling exponent values, it may be possible to identify the main growth mechanisms involved in GDOES erosion of the target surfaces.

To identify the operating mechanisms leading to a given set of scaling exponents, these values are usually compared with those obtained from stochastic growth (etching) equations. For erosion systems, including ours, where an initial morphological instability (characterized by a sharp roughness increase) takes place, the most basic continuum equation describing the surface morphology dynamics is:

$$\partial_t h(\boldsymbol{r},t) = \nu\nabla^2 h - k\nabla^4 h + \lambda(\nabla h)^2 + \eta \quad (3)$$

where $\partial_t h$ is the temporal derivative of h, and η is the stochastic noise accounting for the random character of the Ar^+ ions impinging on the target surface (see [29] for a detailed explanation). When ν is negative, the first term on the right side of Eq. (3) is related to the dependence of the erosion rate on the local surface curvature [35, 36]. In contrast, when ν is positive, this term is related to the so-called Edwards–Wilkinson (EW) growth mode [37], which, in this context, would be associated with the opposite effect, i.e., the preferential erosion of surface protrusions. In fact, for GDOES, preferential sputtering of surface ridges caused by the enhanced ion flux has been proposed [11, 28]. The second term is related to surface relaxation through thermal diffusion or ion-induced surface relaxation processes [29]. These two terms define a linear unstable equation that would lead to a continuous and steep roughness increase. However, as the surface roughens non-linear terms appear and begin to increase their relative weight. The first to appear is the third term, known as the KPZ term [38, 39], which in this context is related to lateral erosion processes [35]. This term has a stabilizing effect because it slows down the initial abrupt increase of roughness. The so-called KPZ growth/erosion mode should, in principle, be the most frequently observed [39]; however, this is not the case, and the reason for this is the subject of much debate [39]. In the context of ion erosion of surfaces, this type of scaling has been proposed to appear for ion-beam incidence angles close to the perpendicular to the target surface and at large length and time scales [40]. However, also in the context of ion sputtering, KPZ scaling is experimentally elusive.

Finally, it is important to note that in equations like (3), the value of the coefficients of the different terms is very important. For example, depending on their relative weight, one scaling region may start earlier and last longer. In the context of ion erosion much effort has been made to determine their dependence on experimental variables [35] including the ion flux, sputtering rate, temperature, angle of ion incidence, and the characteristics of the ion cascade, in particular the penetration length and the lateral and longitudinal straggling [41–43].

Results and discussion

Surface dynamics of monoelemental films under GDOES

As commented above, the first step in rigorously characterizing the effect of GDOES on the analysed surface and, in particular, its roughness was studying the morphology of both Cr and Ti thick films over increasing exposure times. Figure 1 presents the changes in surface roughness, obtained using AFM imaging, with GDOES sputtering time. Despite quantitative differences, the surface roughness has a similar trend for both samples. There is an initial smoothening of the deposited

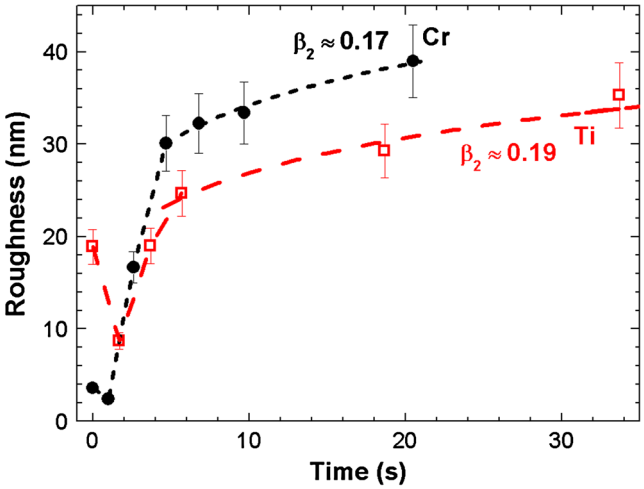

Fig. 1 Temporal evolution of surface roughness during GDOES sputtering of chromium and titanium single layers. The growth exponents β_2 were calculated for times>6 s

roughness during the first 2 s of sputtering, followed by a sharp roughness increase for $t<10$ s. For longer sputtering times the roughness continues increasing with time, but at a much slower pace. A crucial property of the irradiated surface in relation to the GDOES process is its sputtering yield, which is substantially higher for Cr than for Ti (see Table 1) [23]. We discuss the main results obtained for both systems below.

Figure 2 shows the characteristic AFM images of the different temporal stages of GDOES irradiation of the Cr film. The initial morphology corresponds to the as-grown film (Fig. 2a), which is granular. Its roughness (σ=3.6 nm) is defined mostly by the average grain size, because no relevant height fluctuations are observed for length scales larger than this. The grain size has a relatively wide distribution, with values in the 70–120 nm range. However, just after 1 s of GDOES sputtering (corresponding to a sputtering depth of approximately 40 nm), the granular morphology has vanished (Fig. 2b) and the surface has become smoother (σ=2.4 nm). As GDOES continues, until 5 s of radiation the surface roughens sharply (σ~30 nm), increasing its roughness by one order of magnitude (Fig. 1) and developing a characteristic morphology defined by small depressions or holes that coarsen with irradiation time (Fig. 2c). From this stage on (Fig. 2d–e) the surface roughness keeps increasing, but at an appreciably slower pace $\sigma \propto t^{0.17}$ (Fig. 1). Finally, at the longer irradiation stages (t>22 s), the Si surface is reached and the morphology changes markedly, becoming quite inhomogeneous (these data are not shown because they will be studied in an upcoming article).

Further information on the surface morphology dynamics can be obtained from the evolution of the corresponding PSD functions, displayed in the logarithmic scale of Fig. S2 (Electronic Supplementary Material). First, it is worth noting the differences between the PSD of the initial Cr film surface and

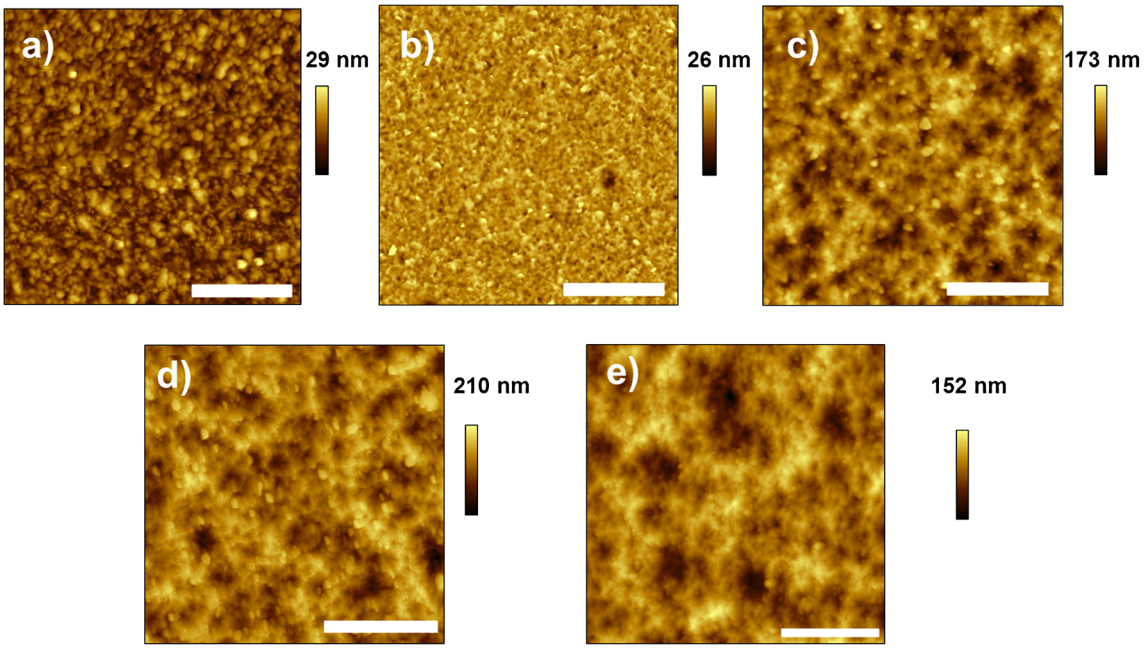

Fig. 2 AFM images obtained for the Cr initial surface (**a**), and after GDOES irradiation for 1 s (**b**), 5 s (**c**), 10 s (**d**), and 20.5 s (**e**). The scale bars correspond to 1.1 μm (**a**) and 2 μm (**b**–**e**)

that corresponding to 1 s of irradiation. Clearly, the latter lies below the initial one, in agreement with the observed roughness reduction. Moreover, the roughness is reduced at all length scales (i.e., for the whole k range sampled), which agrees with the vanishing of the marked initial granular morphology. As noted before, the surface undergoes a sharp change after 3 s of irradiation: the PSD shifts upwards for all k, in agreement with the observed roughness increase. This behaviour could correspond, in principle, to a different type of scaling, known as intrinsic anomalous [44]. It has been suggested that it is related to non-local effects during surface dynamics [45]. However, after 5 s a clear regime appears in which all PSD curves overlap, with a neat linear regime in which α_1=0.7; this starts to develop at t=3 s, and is well defined for k values in the 0.006–0.002 nm^{-1} range (i.e. for length scales in the 150–500 nm range). When t=10 s a second scaling regime appears for smaller k values (length scales larger than 500 nm), characterized by α_2=0.39. This regime is extended towards smaller k values (larger length scales) as the irradiation time increases to t=20.5 s. We can estimate the value of the coarsening exponent from the change with time of the crossover k_c value. This analysis yields a relation $1/z_2 \sim 0.4 \pm 0.1$ but it should be noted that the error involved is relatively large because the estimation is not direct. Accordingly, the surface dynamics in the 5–20.5 s range have the scaling exponents $\beta_2 = 0.17 \pm 0.06$, $1/z_2 \sim 0.4 \pm 0.2$, and $\alpha_2 = 0.39$, which obeys, within the error bars, the relationship $1/z = \beta/\alpha$ [29], related to a kinetic roughening process.

There are problems associated with the PSD analysis of systems, including that addressed in this work, which have several scaling regions, each operating at different lengths (i.e., different k windows) and temporal scales. In consequence, both the temporal and length windows to define the corresponding exponent values become rather short, which impedes precise determination. In our case, another problem affecting determination of the exponents is the speed of the GDOES process: a 3 μm-thick layer can be etched in less than 1 min. These problems would mostly affect determination of the β and $1/z$ exponents, because the sampling involved is lower than that for determination of α from the PSD curves.

A similar analysis can be performed for the irradiated titanium films. Typical AFM images of the induced morphologies are displayed in Fig. 3. The initial morphology is also granular (Fig. 3a), but now the grain structure alone does not determine the surface roughness because there are clear height fluctuations for length scales larger than the grain size, which is related to a specific grain aggregation that leads to the formation of surface protrusions and depressions. This initial surface is substantially rougher (σ~19 nm) than that of the Cr system, for which σ<4 nm. The grain size has a relatively wide distribution, with values in the 120–200 nm range: larger values than those for the pure Cr system. In the early stages of the GDOES process (t=2 s) the surface is smoothed to a large extent with respect to the Cr system, with σ<9 nm. The granular morphology is mostly erased and, at the same time, the morphology characterized by surface depressions or holes, already obtained on the Cr system, is developing (Fig. 3b). As the process proceeds (t=4 s) this morphology becomes more marked (Fig. 3c) and the roughness increases abruptly (Fig. 1), as for the Cr system, attaining a value close to the

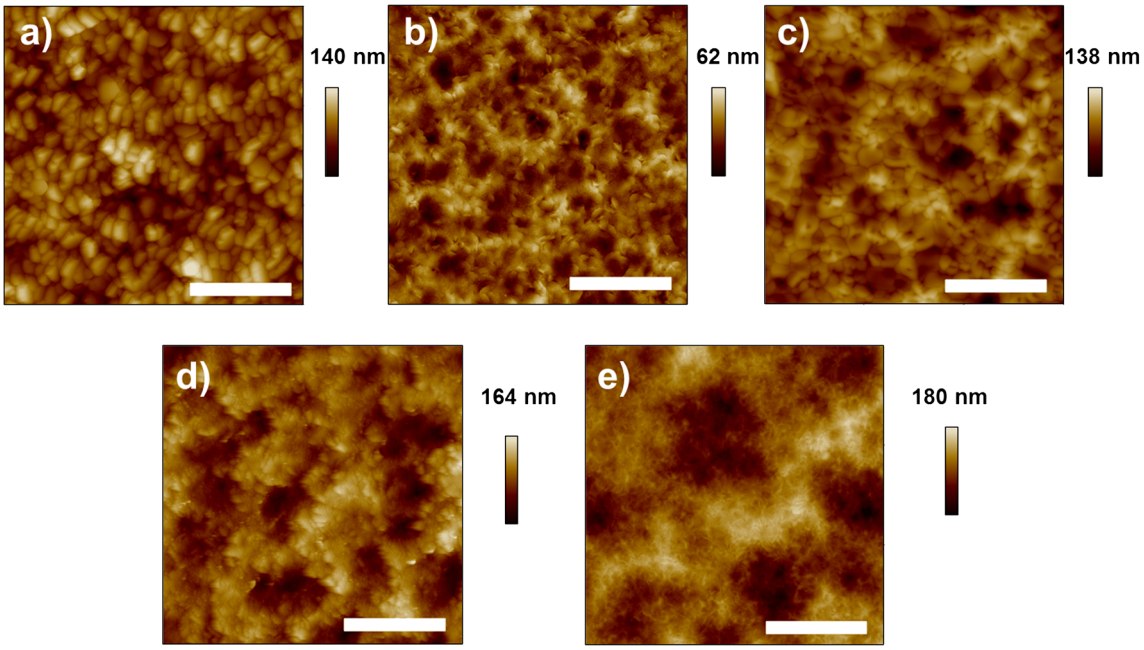

Fig. 3 AFM images obtained for the Ti initial surface (**a**), and after GDOES irradiation for 2 s (**b**), 4 s (**c**), 6 s (**d**), and 34 s (**e**). The scale bars correspond to 1.1 μm (**a**) and 2 μm (**b**–**e**)

initial one (σ=19 nm). At t=6 s, σ=25 nm and the hole morphology is homogeneously found on the surface, together with some texturing of the surface probably related to Ti polycrystallinity (Fig. 3d). From this stage on, the σ increase is much slower, and $\sigma \propto t^{0.19}$. The morphology evolves in such a way that while the surface depressions coarsen with time they become more blurred and less marked (Fig. 3e). At the same time, clear height fluctuations encompassing several of these depressions start to develop, becoming more marked and larger in lateral size with time. However, the initial roughness evolution is very similar to that observed for Cr, despite the different initial film roughness and sputtering yields.

The corresponding PSD evolution of titanium surfaces is shown in Fig. S3 (Electronic Supplementary Material). The PSD of the initial surface lies above those measured for the irradiated surfaces for k>0.0013 nm^{-1} (i.e., length scales smaller than 750 nm). This means that the ion irradiation smoothes the surface at short length scales and roughens it at long scales. As the irradiation proceeds, a clear linear regime develops, again with α_1=0.7, the same value obtained for the Cr system. For long irradiation times, a new linear region appears for very small k values (lengths longer than 1.8 μm). Because of its shortness it is difficult to accurately determine the slope, but it seems consistent with $\alpha_2 \sim 0$. Accordingly, the determination of the coarsening of this late regime is quite ambiguous (see inset of Fig. 3), being $1/z_2$= 0.6±0.2. Thus, the scaling exponents are β_2=0.19±0.09, $1/z_2$=0.6±0.2 and $\alpha_2 \sim 0$.

From these results it is evident that the surface morphology evolution of Ti and Cr films under GDOES has some common features. The first is the initial smoothening of the surface within the very first moments of irradiation, which erases the granular film surface structure and produces a rather featureless morphology. This roughness reduction is more marked for Ti (from 19 nm to 9 nm) than Cr (from 3.6 nm to 2.4 nm) and is substantial, being in the range 33–55 %. A similar initial surface smoothening has been observed for aluminium oxide films under similar GDOES conditions [28]. Only after this initial smoothening does the surface undergo a rapid roughening; this occurs in both systems, with quite similar quantitative dynamics (i.e., both with α_1=0.7). This steep roughening is explained by the dominance of the linear terms in the corresponding surface erosion continuum equation, which leads to a continuous surface roughening. Despite the different initial surface roughness, both systems behave similarly up to this stage. This likeness suggests that these trends are characteristic of the GDOES process.

Regarding depth profiling studies, it has been proposed that the ion-induced surface roughness depends on the relative value of the grain or column (if the film has a columnar growth morphology) size and the sputtered depth [46]. Thus, for a sputtered depth smaller or larger than the grain size, relationships of $\sigma \sim t$ or $\sigma \sim t^{0.5}$ are expected, respectively [47, 48]. This behaviour is predicted on the basis of the roughening caused by the differences in sputtering rates obtained on differently oriented crystallographic surfaces, and it has been observed for metallic multilayers under AES depth profiling [49]. In our GDOES system, we have obtained a behaviour that is partially similar to these predictions. Thus, after the initial GDOES-induced smoothening, there is indeed a regime in which the

roughness increases steeply, compatible with a linear dependence on the erosion time, for both Cr and Ti films. However, for Ti this regime lasts until an etched depth of approximately 350 nm, i.e., close to the Ti surface grain size, whereas for Cr it is extended to even greater depths of ~400 nm, a value clearly higher than the Cr surface grain size. Finally, the second roughening regimes observed for both systems have a quite similar dependence of $\sigma \sim t^{0.18}$, which is quite different from that expected. There are two reasons why the observed behaviour is not quantitatively equal to the expected behaviour. First, the grain and column size usually increase with growth time for different deposition techniques [29, 50, 51]. This implies that the spatial distribution of the local sites with different sputtering rates should change with sampled depth, which was not considered in the model. Second, the ion incoming geometry in GDOES depth profiling is more isotropic than in standard AES depth profiling, in which the ion impinging incidence is relatively directional [8]. However, the observed behaviour in our system is qualitatively consistent with the expected sequence of steep and slower roughening predicted by this model.

The differences between the systems appear once the initial roughening ends and the final scaling regime begins, i.e., for relatively long length scales. For Ti, the surface roughens less than for Cr, for which the sputtering yield is larger and the erosion proceeds at a faster pace. In fact, as can be observed from the corresponding PSDs (Fig. S3, Electronic Supplementary Material), the second regime practically appears for the two last sampled data, i.e. for length scales larger than 1.8 μm (very small k values). The corresponding scaling exponents ($\alpha_2 \sim 0$, $\beta_2 \sim 0.19$, and $1/z_2 \sim 2/3$) are not compatible with any known model. However, as noted previously, the most reliable determination could be that of the α exponent, whose value could suggest an EW scaling behaviour [37] that predicts $\alpha_2 \sim 0$, $\beta_2 \sim 0$, and $1/z_2 \sim 0.5$. It should be noted that in this case the roughness scales logarithmically with both time and length, leading to the zero values of α and β. However, the poor sampling of this regime should be stressed.

Despite this problem, it is clear from comparison of the surface dynamics that they are indeed different, particularly at longer lengths and always above the 500 nm range, which is well above the initial surface grain size. In the Cr system, a long length regime characterized by $\alpha_2 = 0.39$, $\beta_2 \sim 0.17$, and $1/z_2 \sim 0.42$ is observed. Taking into account the error bars, the data sampling, and the greater reliability of the α determination, these values are very close to those of the KPZ model in 2+1 dimensions [38]. It is interesting that this regime is attained for the system (Cr) that is farther from equilibrium, because the sputtering rate is higher and the roughening is steeper, leading to earlier formation of higher slopes on the surface and thus enhancing the appearance of the non-linear regimes (the KPZ term being the first one). In a recent publication, Nicoli et al. [52] proposed that the relative weight of the KPZ term is proportional to the ratio λ^2/ν^3 under similar experimental conditions as in our case. For lower values of this ratio an EW scaling is predicted, whereas for high values KPZ scaling is expected. As commented in the introduction, both λ and ν are material-dependent coefficients. In particular, they depend on the sputtering rate and penetration length and on the lateral and longitudinal straggling of the ion impacts. It is therefore not surprising that the surface dynamics for the systems are different, because the values of λ and ν will be different. Finally, the results obtained in these experiments regarding the asymptotic KPZ regime may help in planning future experiments studying dynamic scaling in ion-sputtered surfaces. So far, KPZ scaling has been elusive in ion-beam sputtering experiments in which an ion beam impinges on the target surface. These beams, although they can be relatively wide, retain a more-or-less defined angle of incidence. In contrast, in GDOES the ions probably impinge with a very wide-angle distribution [8]. Accordingly, to find the predicted KPZ scaling it could be informative to design set-ups with a wide incidence-angle distribution and to irradiate target materials with a high sputtering yield, as for Cr.

As noted before, the KPZ term is a high-order one in Eq. (3) and, therefore, becomes important when the local slopes are greater. It is therefore interesting to study whether the Cr eroded films (for which strong signatures of the KPZ scaling regime appear) effectively present higher slopes than the Ti ones (for which KPZ regime has not appeared in the temporal window sampled). We thus obtained, by means of the AFM software, the slope distribution of these surfaces after prolonged GDOES erosion (i.e. 20.5 s for Cr and 34 s for Ti). These distributions are displayed in Fig. 4. The slope distribution of Ti is clearly narrower than that of Cr, in which

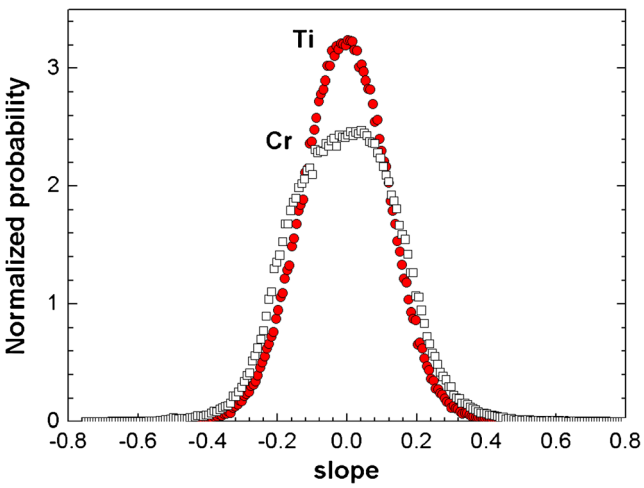

Fig. 4 Normalized slope distributions, obtained from the corresponding AFM images, for the pure Cr and Ti surfaces after 20.5 s and 34 s, respectively; i.e., after the GDOES-induced first steep surface roughening regime. Note the wider slope distribution for the Cr system, indicating that larger surface slopes develop

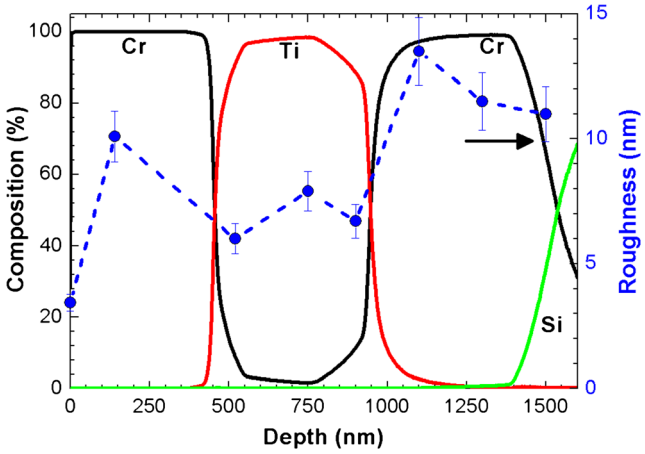

Fig. 5 Evolution of roughness with sputtering depth for the Cr–Ti–Cr trilayer system. The quantified GDOES composition depth profile has been overlapped with the roughness profile to correlate the observed changes

larger slopes are developed. This result is consistent with the scaling analysis described above, despite the limitations already mentioned.

Surface dynamics of multilayer Cr–Ti films under GDOES irradiation

Once we had studied the surface dynamics of monoelemental chromium and titanium films under GDOES, we could address a similar analysis of multilayer Cr–Ti systems.

First, we irradiated a 1.5 μm multilayer Cr–Ti–Cr film formed of three 0.5 μm layers, two of chromium and an intermediate of titanium, deposited on a silicon (100) substrate. Figure 5 shows the quantified GDOES depth profile of the multilayer [23]. The GDOES profile has been overlapped with the roughness changes with depth, as measured by AFM. Figure 6 shows the AFM images corresponding to the most representative stages of the surface evolution. In each case it is indicated which material, Cr or Ti, is mainly being sputtered away. Before irradiation (see Fig. 6a) the Cr top-layer surface has the characteristic granular morphology already observed for the pure Cr films (σ=3.4 nm in Fig. 5). After 4 s of irradiation, and before the Cr top layer has been completely etched, the porous and rough morphology observed for the pure Cr system is again observed (Fig. 6b), with a substantial roughness increment of up to σ=10 nm (see Fig. 5). After a further 5 s sputtering the top Cr layer has been sputtered away and the ions impinge on the intermediate Ti layer. This change of material leads to a change in the surface morphology (Fig. 6c), which becomes smoother (σ=5.8 nm in Fig. 5). In addition, the porous features of the morphology are now blurred or less clear, which agrees with the results obtained for the pure Ti system. Similar morphologies and surface roughness values, in the 5.8–8 nm range, hold throughout the etching of the Ti layer until, at 17 s, the second Cr layer is reached. This second change of material causes an abrupt roughness increment up to σ=14 nm (Fig. 5) and the reappearance of clearer hole features on the surface (Fig. 6d). The corresponding PSD functions are displayed in Fig. S4 (Electronic Supplementary Material). After 4 s, when the Cr layer is being etched, the PSD lies above that corresponding to the initial surface for $k<0.01\ \mathrm{nm}^{-1}$, that is, for length scales larger than 100 nm. In addition, a linear region is again observed,

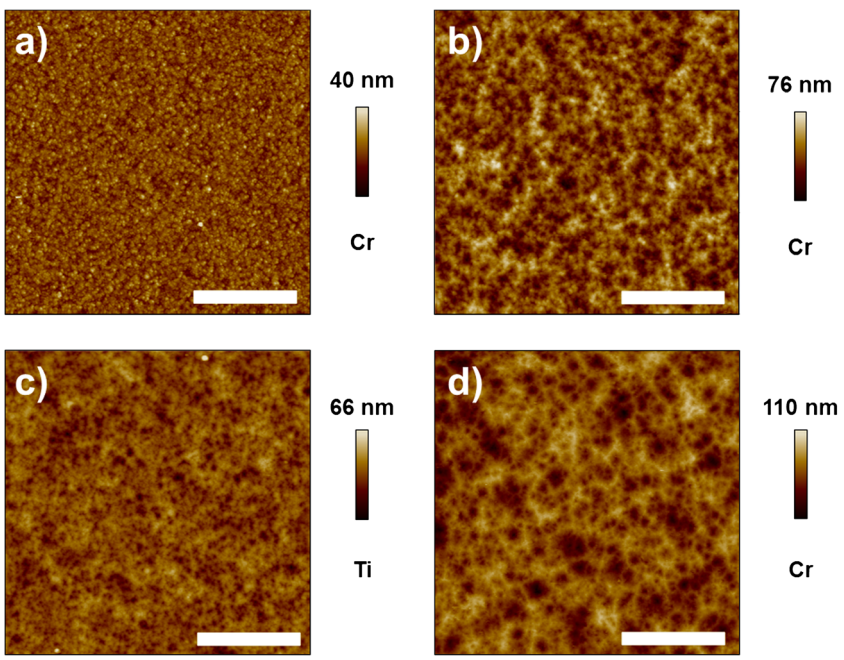

Fig. 6 AFM images obtained for the Cr–Ti–Cr trilayer initial surface (**a**), and after GDOES irradiation for 4 s (**b**), 9 s (**c**), and 17 s (**d**). The scale bars correspond to 2 μm

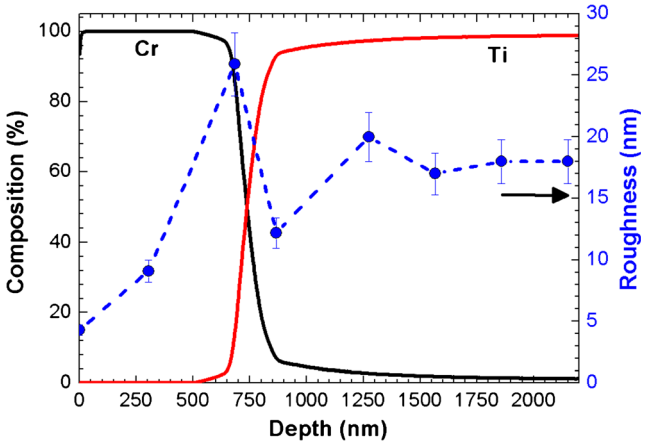

Fig. 7 Evolution of roughness with sputtering depth for the Cr–Ti thick bilayer system. The quantified GDOES composition depth profile has been overlapped with the roughness profile to correlate the observed changes

with α_1=0.7 for 0.003<k<0.008 nm^{-1}, which is consistent with that observed for the Cr system. This behaviour implies that irradiation induces roughening at larger scales. In contrast, when the ions have etched the top Cr layer and are impinging on the Ti atoms (t=9 s), the roughness decreases abruptly, shifting the PSD downwards with respect to that obtained at 4 s. In fact, the new PSD lies below the former one for the whole k range sampled, indicating that this smoothening takes place at all sampled length scales. The linear regime with α_1=0.7 has been appreciably shortened, and a new linear region with α_2~0 for 0.0015<k<0.066 nm^{-1} can be identified. Finally, after 17 s, when the ions have reached the bottom Cr layer, the roughness increases again and the corresponding PSD practically overlaps that obtained after 4 s for k>0.003 nm^{-1}. For 0.001<k<0.003 nm^{-1} a new regime can be clearly discerned with α_2=0.39, as was obtained for the pure Cr system.

We then studied a 3.0 μm Cr–Ti bilayer film, formed of a 0.75 μm Cr top layer and a thicker 2.25 μm Ti film deposited on a silicon (100) substrate. Figure 7 shows the quantified GDOES depth profile of the Cr–Ti bilayer [23]. The GDOES profile has been overlapped with the roughness changes with depth, as measured by AFM. The representative AFM images of the etching process are shown in Fig. 8. From the initial granular morphology of the Cr top-layer (see Fig. 8a), with σ=4.3 nm, the first 9 s of GDOES sputtering, during which this layer is being etched, leads to the development of a rough morphology with σ=26 nm (Fig. 7). This morphology is characterized by a layer of clear pore and/or depressions features (see Fig. 8b), as was detected when irradiating the pure Cr film. From this stage on, the Ti middle layer begins to be etched. In this range, the surfaces are smoother and are characterized by morphologies akin to those obtained for the pure Ti system (see Fig. 8c–d). Thus, at the Cr–Ti interface the surface roughness drops to a value of 12 nm, with a slow increase as the sputtering of the Ti layer proceeds, up to a saturation value in the 17–20 nm range (Fig. 7). The PSD evolution (Fig. S5, Electronic Supplementary Material) is somewhat different from that observed for the thin Cr–Ti–Cr trilayer. Because of the marked roughening induced by the ions during the first 9 s of sputtering, the corresponding PSD is substantially shifted upwards with respect to that of the

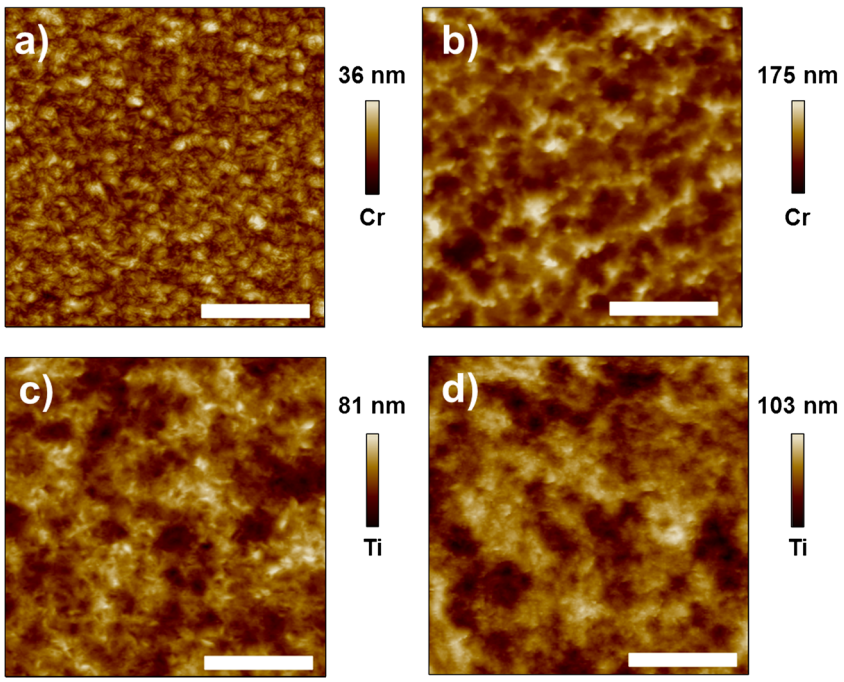

Fig. 8 AFM images obtained for the thick Cr–Ti initial surface (**a**), and after GDOES irradiation for 9 s (**b**), 12 s (**c**), and 34 s (**d**). The scale bars correspond to 2 μm

initial surface, for the whole k window. A short linear regime, with α_2=0.39, has already appeared around k~0.001 nm^{-1}. Once the Ti layer is reached (after 12 s) the roughness decreases abruptly, and the PSD clearly lies below that obtained for the top Cr layer (9 s). In addition, a clear and extended linear regime (α_1=0.7) for 0.001<k<0.01 nm^{-1} has developed. As the sputtering proceeds in the same thick Ti layer, the PSD evolves as it did for the pure Ti system, with subsequent PSD mostly overlapping with the previous ones and with the linear regime extending further, towards smaller k values.

The most striking result obtained for the Cr–Ti bilayer and the Cr–Ti–Cr trilayer is the induced surface roughness decrease, caused by the inclusion of a buried Ti layer at the interface below the top Cr film (Figs. 5 and 7). Both configurations lead to roughness values smaller than those of the pure Cr and Ti systems. In particular, when the initial Cr layer is thicker (Cr–Ti bilayer) the final roughness decreases by a factor higher than two, from σ=26 nm at 9 s to σ=12 nm at 12 s (Fig. 7). This is caused by the steep roughness increase occurring during the first stages of the irradiation (from 4.3 up to 26 nm), already observed for the pure systems: when the underneath Ti layer was finally reached the previous erosion of the thick top Cr layer had already led to an important surface roughening. This trend is confirmed for the trilayer system, for which the middle Ti layer is reached before 9 s of irradiation. At this stage, σ drops from a value of 10 nm, attained after 4 s when the Cr top layer was being etched, to just 5.8 nm. Therefore, the highest roughness achieved when irradiating the first Cr layer is smaller than that obtained for the bilayer, because the Cr layer was thinner. These data reveal that the inclusion of a buried Ti layer under the top Cr layer significantly reduces the surface roughness at the interface. Furthermore, the data obtained for the trilayer also reveal that when the intermediate Ti layer is etched away and the bottom Cr layer is reached, the roughness increases again substantially (from σ=6.6 nm at 15 s to 14 nm at 17 s) at this second interface. These results indicate that, by appropriate placing of a buried layer of a material with a lower sputtering yield, a substantial decrease of GDOES-induced roughness can be achieved. Furthermore, Figs. 5 and 7 prove that the depth location of this layer is a crucial variable in further decreasing this roughness. Therefore, appropriate choice of material (i.e. sputtering yield values) combination and their depth of location can substantially control the surface roughness induced by GDOES.

A possible explanation for this behaviour may be related to the combination of layers of elements with a significant difference in sputtering yields, as for Cr and Ti. During the irradiation of the top Cr layer (the one with the higher sputtering yield) the roughness initially increases steeply, similarly to that seen during irradiation of the single Cr layer. However, as explained above, the inclusion of an underlying Ti layer with a lower sputtering yield reduces the surface roughness of both the thick bilayer and thin trilayer systems. Thus, when the ions are irradiating the Cr layer and the buried Ti atoms begin to be sputtered at the minima of the surface, the progress of the roughening is somehow frozen at the deepest locations of the Ti atoms with respect to those parts still lying in the Cr layer. As a consequence, the interface roughness decreases. Interestingly, the slope distribution of the eroded surface for each layer, either Cr or Ti, corresponds to that obtained for the respective pure homogeneous film. Figure 9 displays the normalized slope distributions from 14 μm-wide AFM images for the bilayer system irradiated during 9 s (top Cr layer) and 12 s (underlying Ti layer). The distribution of the 12 s sample is clearly narrower, in agreement with the

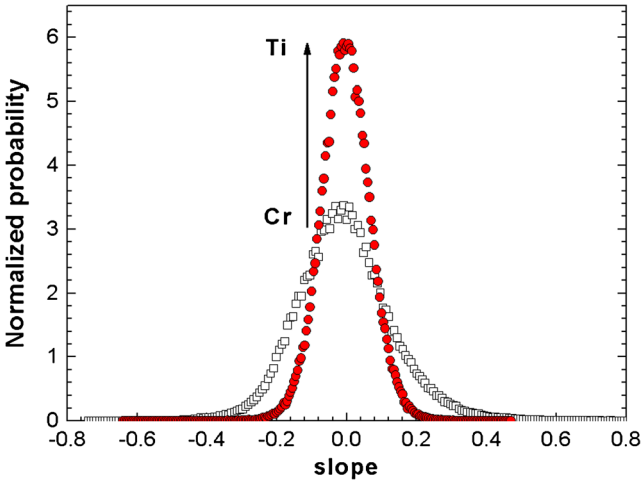

Fig. 9 Normalized slope distributions, obtained from the AFM images, for the Cr–Ti thick bilayer system after 9 s (Cr) and 12 s (Ti) of sputtering. The arrow indicates the change of material during the sputtering. Note how the slope distribution depends on the nature of the sputtered metal

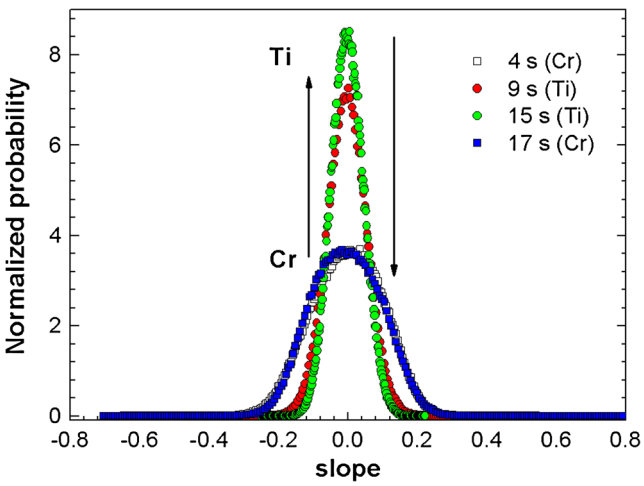

Fig. 10 Normalized slope distributions, obtained from the AFM images, for the Cr–Ti–Cr trilayer system after 4 s (Cr), 9 s and 15 s (Ti), and 17 s (Cr). The arrows indicate the change of material during the sputtering. Note how the slope distribution depends on the nature of the sputtered metal

roughness decrease. The same behaviour is obtained for the slope distribution in the thin trilayer system (Fig. 10). Initially, when the Cr top-layer is being sputtered (4 s), the slope distribution is relatively wide. However, once the middle Ti layer is reached (9 s) the slope distribution becomes narrower. While the Ti layer is being eroded, up to 15 s, the same narrow slope distribution holds. Finally, when the second Cr layer is reached (after 17 s), the distribution becomes wider, being quite similar to that observed when the top Cr layer was eroded. In this case, when the ions start to sputter the underlying Cr atoms, the roughening at these places advances faster, leading to increased roughness and to the development of higher slopes.

The data obtained for these systems (Figs S4 and S5, Electronic Supplementary Material) also reveal that the PSD curves obtained for each layer correspond to those obtained for the respective pure systems. This is better observed when a Cr layer is being sputtered: in these cases, a short but clear KPZ scaling region is observed for large length scales, in agreement with the results obtained for the Cr film. The same behaviour is harder to detect for the Ti layers, because the scaling regime at these long scales was already difficult to observe on the Ti film. However, these results confirm that the scaling properties observed for each pure system are truly characteristic of each material. Therefore, the GDOES-induced surface morphology has important contributions from the target material properties.

Conclusions

We studied GDOES-induced surface roughening of single metal (Cr, Ti) layers and Cr–Ti and Cr–Ti–Cr multilayers. This study was performed by analysing, by use of AFM, the surface morphology of the centre of the main crater produced, at different process times. Data relating to the temporal and spatial roughness correlation were analysed under the framework of the dynamic scaling theory. From the experiments performed on the single layers, we can conclude that a similar temporal dynamic is observed for both materials. Thus, after initial surface smoothening, there is a regime in which the roughness increases sharply to reach a final regime where $\sigma \sim t^{0.18}$ for both systems. However, the crossover between the regimes is different for each material. A more detailed analysis of the scaling properties of the final temporal regime proves that a particular scaling appears for each system at large length scales. For Cr the surface-etching scaling follows the KPZ model, whereas for Ti an EW scaling regime is suggested. The former is related to lateral erosion processes (i.e. erosion along the locale normal to the surface), whereas the second one is related to preferential erosion of surface protrusions. These different scaling properties are consistent with the development of higher surface slopes for the Cr system. Finally, for the multilayer systems, a clear decrease in the induced roughness is achieved when the underlying Ti layer is reached. This lower roughness value persists throughout the erosion of the Ti layer. Therefore, for practical GDOES analysis, the results of this work reveal how GDOES-induced surface roughness can be tuned by choosing materials with the appropriate combination of properties, in particular their sputtering yields, and by the appropriate depth location of the material with the lower sputtering yield. Moreover, these results could be useful for designing and interpreting GDOES experiments on multilayer targets in the sub-micrometric range.

Acknowledgments The authors thank R. Cuerno for fruitful discussions. This work has been partially supported by Ministerio de Economía y Competitividad (projects FIS2012-38866-C05-05, CSD2008-00023 and RyC2007-0026).

References

1. Winchester MR, Payling R (2004) Radio-frequency glow discharge spectrometry: a critical review. Spectrochim Acta Part B 59:607–666
2. Bings NH, Bogaerts A, Broekaert JAC (2008) Atomic spectroscopy. Anal Chem 80(12):4317–4347
3. Bubert H, Grallath E, Quentmeier A, Wielunski M, Borucki L (1995) Comparative investigation on copper oxides by depth profiling using XPS, RBS and GDOES. Fresenius J Anal Chem 353:456–463
4. Oswald S, Baunack S (2003) Comparison of depth profiling techniques using ion sputtering from the practical point of view. Thin Solid Films 425:9–19
5. Thobor A, Rousselot C, Mikhailov S (2003) Depth profiles study of n(TiN+AlN) bilayers systems by GDOES and RBS techniques. Surf Coat Technol 174–175:351–359
6. Escobar Galindo R, Gago R, Lousa A, Albella JM (2009) Comparative depth profiling analysis of nanometre metal multilayers by ion probing techniques. Trends Anal Chem 28(4):494–505
7. Escobar Galindo RE, Gago R, Duday D, Palacio C (2010) Towards nanometric resolution in multilayer depth profiling: a comparative study of RBS, SIMS, XPS and GDOES. Anal Bioanal Chem 396: 2725–2740
8. Klemm D, Hoffmann V, Wetzig K, Eckert J (2009) DC- and RF-GD-OES measurements of adsorbed organic monolayers on copper. Anal Bioanal Chem 395(6):1893–1900
9. Beck U, Reiners G, Wirth T, Hoffmann V, Präßler F (1996) Multilayer reference coatings for depth profile standards. Thin Solid Films 290–291:57–62
10. Shimizu K, Habazaki H, Skeldon P, Thompson GE (2003) Impact of RF-GDOES in practical surface analysis. Spectrochim Acta Part B 58:1573–1583
11. Shimizu K, Habazaki H, Skeldon P, Thompson GE (2003) Radiofrequency GDOES: a powerful technique for depth profiling analysis of thin films. Surf Interface Anal 35:564–574
12. Pisonero J, Fernández B, Pereiro R, Bordel N, Sanz-Medel A (2006) Glow discharge spectrometry for direct analysis of thin and ultra-thin solid films. Trends Anal Chem 25:11–18
13. Escobar Galindo R, Forniés E, Gago R, Albella JM (2006) Nanometric resolution in glow discharge optical emission spectroscopy and Rutherford backscattering spectrometry depth profiling of metal (Cr, Al) nitride multilayers. Spectrochim Acta Part B 61(5): 545–553

14. Quentmeier A (1997) Sections 7.1 and 7.2. In: Payling R, Jones DG, Bengston A (eds) Glow discharge optical emission spectroscopy. Wiley, New York
15. Shimizu K, Habazaki H, Skeldon P, Thompson GE, Marcus RK (2001) Influence of interfacial depth on depth resolution during GDOES depth profiling analysis of thin alumina films. Surf Interface Anal 31:869–873
16. Angeli J, Bengston A, Bogaerts A, Hoffmann V, Hodoroaba V, Steers E (2003) Glow discharge optical emission spectrometry: moving towards reliable thin film analysis: a short review. J Anal At Spectrom 18:670–679
17. Hoffmann V, Dorka R, Wilken L, Hodoroaba VD, Wetzig K (2003) Present possibilities of thin-layer analysis by GDOES. Surf Interface Anal 35(7):575–582
18. Escobar Galindo R, Forniés E, Albella JM (2005) Interfacial effects during the analysis of multilayer metal coatings by radiofrequency glow discharge optical emission spectroscopy: Part 2. Evaluation of depth resolution function and application to thin multilayer coatings. J Anal At Spectrom 20:1116–1120
19. Daughtrey EH Jr, Donohue DL, Slevin PJ, Harrison WW (1975) Surface sputter effects in a hollow cathode discharge. Anal Chem 47: 683–688
20. Bruhn CG, Harrison WW (1978) Sputter-Atomization Studies with a Glow Discharge. Anal Chem 50:16–21
21. Shimizu K, Brown GM, Habazaki H, Kobayashi K, Skeldon P, Thompson GE, Wood GC (1999) Glow discharge optical emission spectrometry (GDOES) depth profiling analysis of anodic alumina films: a depth resolution study. Surf Interface Anal 27:24–28
22. Shimizu K, Brown GM, Habazaki H, Kobayashi K, Skeldon P, Thompson GE, Wood GC (1999) Impurity distributions in barrier anodic films on aluminium: a GDOES depth profiling study. Electrochim Acta 44:2297–2306
23. Escobar Galindo R, Forniés E, Albella JM (2005) Interfacial effects during the analysis of multilayer metal coatings by radio-frequency glow discharge optical emission spectroscopy: Part 1. Crater shape and sputtering rate effects. J Anal At Spectrom 20:1108–1115
24. Oswald S, Hoffmann V, Ehrlich G (1994) Contributions to computer-aided interpretation of ion sputtering depth profiling. Spectrochim Acta Part B 49:1123–1145
25. Präßler F, Hoffmann V, Schumann J, Wetzig K (1996) Quantitative depth profiling in glow discharge spectroscopies: a new deconvolution technique to separate effects of an uneven erosion crater shape. Fresenius J Anal Chem 355:840–846
26. Escobar Galindo R, Albella JM (2008) Modelling of glow discharge optical emission spectroscopy depth profiles of metal (Cr, Ti) multilayer coatings. Spectrochim Acta Part B 63(3):422–430
27. Malherbe J, Martinez H, Fernández B (2010) Donard OFX (2010) Investigation of glow-discharge-induced morphology modifications on silicon wafers and chromium conversion coatings by AFM and rugosimetry. Anal Bioanal Chem 396:2841–2853
28. Trigoulet N, Hashimoto T, Molchan IS, Skeldon P, Thompson GE, Tempez A, Chapon P (2010) Surface topography effects on glow discharge depth profiling analysis. Surf Interface Anal 42:328–333
29. Barabási AL, Syanley HE (1995) Fractal concepts in surface growth. Cambridge University Press, Cambridge
30. Meakin P (1998) Fractals, scaling and growth far from equilibrium. Cambridge University Press, Cambridge
31. Auger MA, Gago R, Fernández M, Sánchez O, Albella JM (2002) Deposition of TiN/AlN bilayers on a rotating substrate by reactive sputtering. Surf Coat Technol 157:26–33
32. Nečas D, Klapetek P (2012) Gwyddion: an open-source software for SPM data analysis, Cent Eur J Phys 10(1): 181–188 (http://gwyddion.net/)
33. Cuerno R, Vázquez L (2004) Advances in Condensed Matter and Statistical Physics. Nova Science, New York
34. Family F, Vicsek T (1985) Scaling of the active zone in the Eden process on percolation networks and the ballistic deposition model. J Phys A 18:L75–L81
35. Makeev MA, Cuerno R, Barabási AL (2002) Morphology of ion-sputtered surfaces. Nucl Inst Methods Phys Res B 197:185–227
36. Bradley RM, Harper JME (1988) Theory of Ripple Topography Induced by Ion Bombardment. J Vac Sci Technol A 6:2390
37. Edwards SF, Wilkinson DR (1982) The Surface Statistics of a Granular Aggregate. Proc R Soc Lond 381:17–31
38. Kardar M, Parisi G, Zhang YC (1986) Dynamic scaling of growing interfaces. Phys Rev Lett 56:889–892
39. Nicoli M, Cuerno R, Castro M (2013) Dimensional fragility of the Kardar-Parisi-Zhang universality class, J Stat Mech: Theory Exp, P11001 (11 pages)
40. Cuerno R, Barabási AL (1995) Dynamic Scaling of Ion-Sputtered Surfaces. Phys Rev Lett 74:4746–4749
41. Sigmund P (1969) Theory of Sputtering. I. Sputtering Yield of Amorphous and Polycrystalline Targets. Phys Rev 184:383–416
42. Castro M, Cuerno R, Vázquez L, Gago R (2005) Self-Organized Ordering of Nanostructures Produced by Ion-Beam Sputtering. Phys Rev Lett 94:016102
43. Muñoz-García J, Cuerno R, Castro M (2009) Coupling of morphology to surface transport in ion-beam-irradiated surfaces: normal incidence and rotating targets. J Phys Condens Matter 21:224020
44. Auger MA, Vázquez L, Cuerno R, Castro M, Jergel M, Sánchez O (2006) Intrinsic anomalous surface roughening of TiN films deposited by reactive sputtering. Phys Rev B 73:045436
45. López JM, Castro M, Gallego R (2005) Scaling of local slopes, conservation laws and anomalous roughening in surface growth. Phys Rev Lett 94:166103
46. Hofman S (1998) Sputter depth profile analysis of interfaces. Rep Prog Phys 61:827–888
47. Wöhner T, Ecke G, Rössler HS (1998) Sputtering-induced Surface Roughness of Polycrystalline Al Films and its Influence on AES Depth Profiles, Surf Interf. Anal 26:1–8
48. Marton D, Fine J (1987) On the development of increasing surface roughness. Thin Solid Films 151:433–439
49. Marton D, Fine J (1990) Sputtering-induced surface roughness of metallic thin films during ion sputtering. Thin Solid Films 185:79–90
50. Vázquez L, Salvarezza R, Herrasti P, Ocon P, Vara JM, Arvia AJ (1995) Dynamic-scaling exponents and the roughening kinetics of gold electrodeposits. Phys Rev E 52:2032–2037
51. Vázquez L, Salvarezza R, Herrasti P, Ocon P, Vara JM, Arvia AJ (1996) Scale-dependent roughening kinetics in vapor deposited gold. Surf Sci 345:17–26
52. Nicoli M, Vivo E, Cuerno R (2010) Kardar-Parisi-Zhang asymptotics for the two-dimensional noisy Kuramoto-Sivashinsky equation, Phys Rev E 82: 045202(R)